JCS ePress online publication date 18 August 2009

Animal cell hydraulics

Guillaume T. Charras[1,2], Timothy J. Mitchison[3] and L. Mahadevan[3,4,5,*]

[1]London Centre for Nanotechnology and [2]Department of Cell and Developmental Biology, Faculty of Life Sciences, University College London, London, WC1H 0AH, UK
[3]Department of Systems Biology, Harvard Medical School, Boston, MA 02115, USA
[4]School of Engineering and Applied Sciences, Harvard University, Cambridge, MA 02138, USA
[5]Organismic and Evolutionary Biology, Harvard University, Cambridge, MA 02138, USA
*Author for correspondence (lm@seas.harvard.edu)

Accepted 13 June 2009
Journal of Cell Science 122, 3233-3241 Published by The Company of Biologists 2009
doi:10.1242/jcs.049262

Summary

Water is the dominant ingredient of cells and its dynamics are crucial to life. We and others have suggested a physical picture of the cell as a soft, fluid-infiltrated sponge, surrounded by a water-permeable barrier. To understand water movements in an animal cell, we imposed an external, inhomogeneous osmotic stress on cultured cancer cells. This forced water through the membrane on one side, and out on the other. Inside the cell, it created a gradient in hydration, that we visualized by tracking cellular responses using natural organelles and artificially introduced quantum dots. The dynamics of these markers at short times were the same for normal and metabolically poisoned cells, indicating that the cellular responses are primarily physical rather than chemical. Our finding of an internal gradient in hydration is inconsistent with a continuum model for cytoplasm, but consistent with the sponge model, and implies that the effective pore size of the sponge is small enough to retard water flow significantly on time scales (~10–100 seconds) relevant to cell physiology. We interpret these data in terms of a theoretical framework that combines mechanics and hydraulics in a multiphase poroelastic description of the cytoplasm and explains the experimentally observed dynamics quantitatively in terms of a few coarse-grained parameters that are based on microscopically measurable structural, hydraulic and mechanical properties. Our fluid-filled sponge model could provide a unified framework to understand a number of disparate observations in cell morphology and motility.

Supplementary material available online at
http://jcs.biologists.org/cgi/content/full/122/18/3233/DC1

Key words: Cytoplasm, Poroelasticity, Cell mechanics

Introduction

Water is required for all life processes, yet its importance in cellular dynamics is often under-appreciated. Its role as a special solvent for biomolecules and salts is well understood (Chandler, 2002), but water is generally consigned to a purely permissive role in cellular events such as signaling, polarization and motility (Alberts et al., 2008). Nevertheless, water plays a crucial role in cell physiology; in plant and fungal cells, water movements are central to growth and motility (Harold, 2002), and classical studies of amoeboid motion have long hinted at roles for water flows in protrusion at the front of motile cells (Allen and Roslansky, 1959). However, since the realization that actin polymerization can drive movement (Theriot et al., 1992; Tilney et al., 1990), the focus of motility research in animal cells has shifted towards a purely cytoskeletal focus. However, recent experiments on actin delivery to the leading edge of a cell (Zicha et al., 2003), spatio-temporally localized cell blebbing (Charras et al., 2005), the role of Na^+/H^+ exchangers and aquaporin channels at the leading edge of cells during motility (Denker and Barber, 2002; Saadoun et al., 2005), and rapid solute movements in cells such as keratocytes (Keren et al., 2008) suggest that cell hydraulics might play an important role in cellular morphology and motility.

Previous experimental work (Charras et al., 2005) lead us to propose that cells could generate transient pressure gradients in the cytoplasm, which we interpreted in terms of a model in which the cytoplasm is a soft, fluid-infiltrated sponge. The physics of such a system can be described using the theoretical framework of poroelasticity, originally established by Biot to describe the mechanics of water-infiltrated soils (Biot, 1941). Experimental and theoretical work by Tanaka and coworkers (Tanaka et al., 1973) and subsequent theoretical extensions by Hui and coworkers (Hui and Muralidharan, 2005) showed that gel mechanics could also be described in the framework of poroelasticity. This framework has the advantage of being simpler and thus more amenable to experimental tests than more complex multiparameter frameworks proposed by others, such as the reactive interpenetrative flow formalism used to model cell motility (Dembo and Harlow, 1986; Herant et al., 2003) or the biphasic theory used to model cartilage mechanics (Gu et al., 1997). Although there is experimental evidence that hydrated collagen gels behave as poroelastic materials (Chandran and Barocas, 2004), no experimental work has directly tested the poroelastic nature of living cells or characterized important parameters such as the pore size of the gel.

Several studies have suggested that cells might be poroelastic (Charras et al., 2008; Charras et al., 2005; Rosenbluth et al., 2008). In the framework of poroelasticity, the cytoplasm is described as a fluid-infiltrated sponge. The solid phase is formed by the cytoskeleton, organelles and lipid vesicles; whereas the fluid phase (cytosol) is composed of water, solutes, and small molecules. One characteristic of such solid-liquid composites is that any deformation applied to them necessitates the redistribution of intracellular fluids, and the time-scale over which this occurs is dictated by the relative ease with which the liquid phase can flow through the pores in the solid phase. This can be expressed by the strain diffusion constant D, with larger strain diffusion constants leading to more rapid fluid redistribution within the cell. This suggests that, if cells

can be described as poroelastic, their well-documented time-dependent mechanical properties (Bausch and Kroy, 2006; Boal, 2002) might arise as a consequence of poroelasticity. For the poroelastic regime to be relevant to biology, movement of water through the cytoplasm would have to be limited at time- and length-scales relevant to biological processes, such as cell migration or cell morphogenesis (typically micrometer length-scales and 10-100 second time-scales).

To directly test the fluid-filled sponge model for an animal cell, we exposed one side of a HeLa cell to a hyperosmotic solution delivered from a micropipette, while the rest was bathed in a flow of normal medium. This removed water from the cell on the side exposed to hyperosmotic medium, but not on the other side (Fig. 1). If the cytoplasm was best described as a viscous liquid, it would have to respond uniformly to this non-uniform stimulus. Conversely, a non-uniform response would support the fluid-filled sponge model. In the latter model, the time-scale for the cytoplasmic response is dictated by how rapidly water can flow through the pores of the sponge-like cytoplasm and can be described using a simplified theoretical analysis within the framework of poroelasticity. Furthermore, if flow through the cytoplasm is slower than flow through the plasma membrane, a gradient in hydration state within the cell becomes possible and this is something that we observe experimentally. Finally, we can infer experimental values for the parameters in a poroelastic model of the cytoplasm and express these in terms of measurable ultrastructural and constitutive cellular parameters.

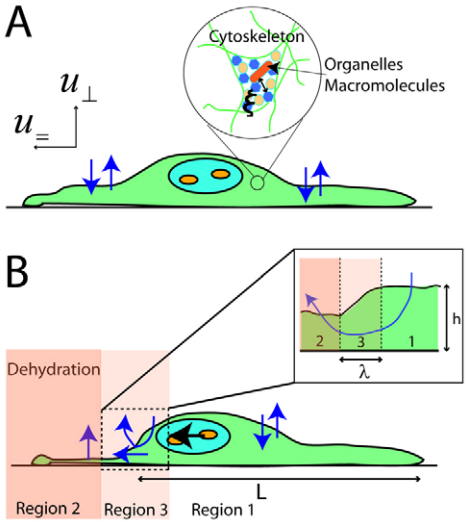

Fig. 1. Experimental setup. (A) In iso-osmotic conditions, water exchanges across the whole of the cell membrane (blue arrows). The cytoplasm is composed of a liquid phase (the cytosol) and a solid phase (the cytoskeleton), which provides a large-pore loose mesh that restricts the diffusion of organelles and macromolecules (ribosomes, polysomes, etc., see inset). The effective pore size for water movement is set both by the cytoskeleton and by macromolecular crowding. Lateral (=) and transversal (⊥) directions referred to in the text are indicated on this graph. (B) When a hyperosmotic medium is locally applied onto the cell, local dehydration ensues (region 2), decreasing cell volume and locally applying stress onto the cytoskeleton. This stress propagates through the cell and eventually causes movement of organelles towards the dehydrated zone (black arrow). In regions close to the dehydration stimulus (region 3), water diffuses from the hydrated to the dehydrated side over a width λ (see inset). $u_{=}$, lateral dimensions of the cell; $u_{\perp}$, perpendicular vertical dimensions of the cell; h, height of the cell; L, lateral dimension of the cell not submitted to dehydration; λ, size of the transition zone between hydrated and dehydrated.

Results

Localised dehydration results in a reversible strain field in the cytoplasm

To locally dehydrate HeLa cells cultured on glass coverslips, we first established a laminar flow of growth medium over the cells while imaging by differential interference contrast (DIC) and fluorescence microscopy. After collecting baseline data, part of the cell (about one third) was exposed for a short time (~2 minutes) to an osmolyte (300 mM of sucrose, mannitol or NaCl were used with similar results) dissolved in medium, using a micropipette (Charras et al., 2005). This treatment locally raised the osmolarity of the medium from ~300 to ~600 mOsm (Figs 1,2; supplementary material Movie 1). Outside the cell, the spatial heterogeneity in solute concentration is maintained by a convective flow at velocity U that competes with solute transversal diffusion over a narrow region with a characteristic length scale D_s/U, where D_s is the solute diffusion constant; on either side of this region (region 3, Fig. 1B), the cell sees a relatively homogeneous osmotic environment.

Application of the external gradient of osmolyte caused objects within the cell to be displaced towards the dehydrated side, which was easily visualized in DIC image sequences (Fig. 2A-C; supplementary material Movies 1,2). We interpret these movements as indicating the generation of a whole-cell intracellular displacement field; the cytoskeleton on the dehydrated side contracts, and the rest of the cell is dragged towards the contracted zone because of cytoskeleton interconnectedness. Movement was reversed after removal of the external osmotic stress (Fig. 2B). To study the dynamics of this process, we tracked fiduciary marks within the cell, typically selecting nucleoli because of their strong optical contrast and constant morphology, over the course of an experiment (Fig. 2B,C). Multiple cycles of dehydration-rehydration subjected the cytoplasm to multiple cycles of displacement-relaxation with near total recovery from one cycle to the next (Fig. 2B,C; supplementary material Movie 1), indicating that the behavior of the cytoplasm over these time-scales is primarily solid-like. During any given cycle, the fiduciary marks approximately followed a one-dimensional trajectory normal to the boundary between the hyperosmotic and isoosmotic regions (Fig. 2C). Dehydration occurred rapidly in the exposed area, as evidenced by rapid cessation of motion of intracellular granules, whereas no change in granule motion was observed on the unexposed side, even after nucleolar movement had ceased (supplementary material Movie 2).

Different hydraulic environments can coexist within a cell separated by a few microns

The difference in movement of cytoplasmic granules between the side of the cell exposed to hyperosmotic solution and the unexposed side suggested that parts of the cell separated by only a few micrometers could exist in different states of hydration. Because the nature of the endogenous cytoplasmic granules was unknown, we repeated the experiment with artificially introduced probes with diameters on the order of the cellular pore size. This was achieved by examining the motion of microinjected quantum dots (QDs) passivated with polyethylene glycol (PEG) [~28 nm diameter including the passivation layer (Derfus et al., 2004; Pons et al., 2006)]. Under control conditions, these QDs diffused freely in the cytoplasm (Fig. 3A; supplementary material Movie 3). When the whole cell was subjected to hyperosmotic shock, the cell volume (V) decreased by 37±14% (n=75 cells, estimated from confocal image stacks) and the QDs stopped moving, presumably because they became trapped within the shrunken cytoplasmic pores (Fig.

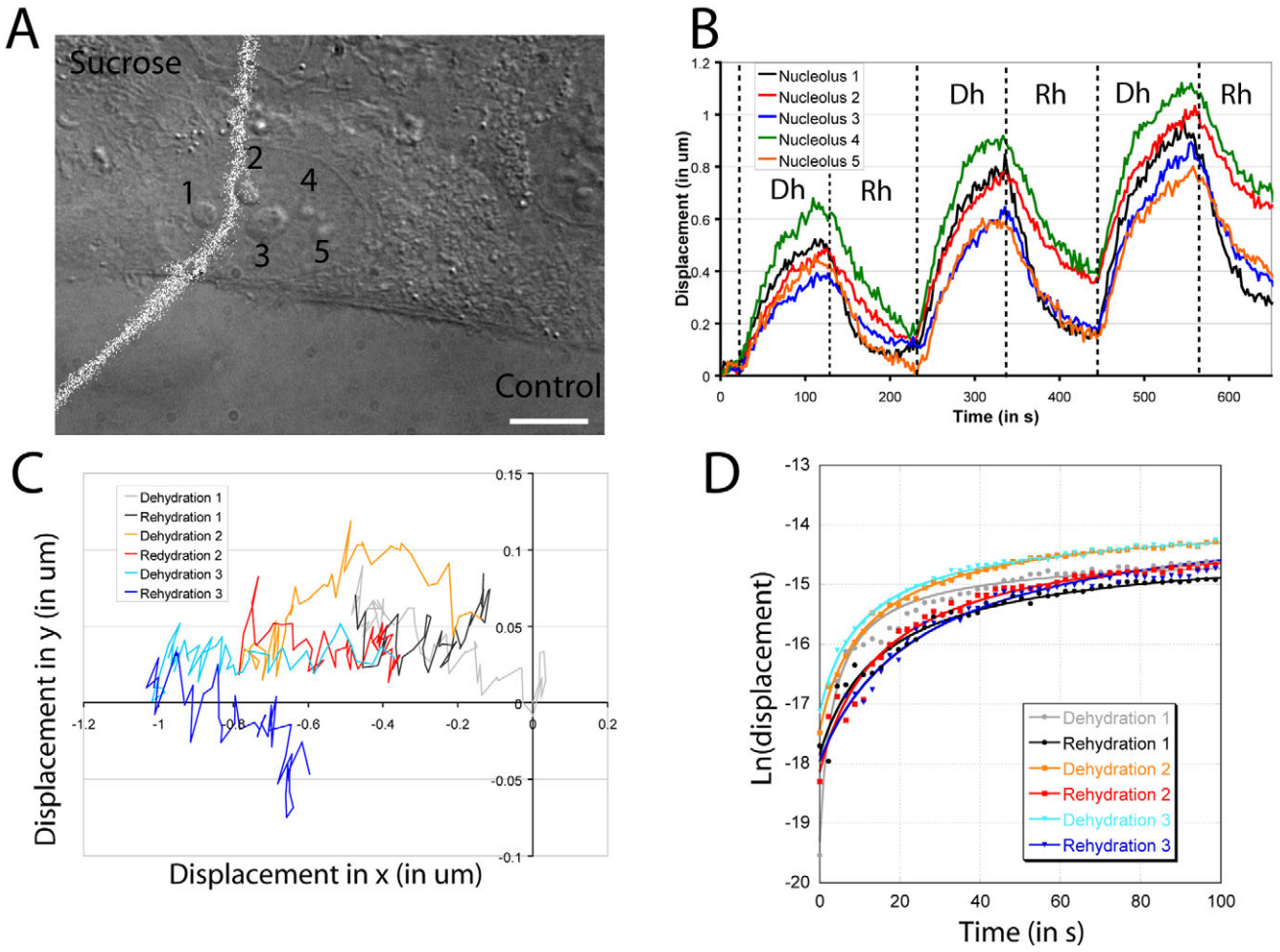

Fig. 2. Dehydration-driven movement of cellular organelles. (A) Differential interference contrast image of a cell with local application of hyperosmotic solution (supplementary material Movie 1). The boundary between the hydrated (control) and dehydrated zone (sucrose) is shown in white and each nucleolus is numbered. Scale bar: 10 µm. (B) Time course of displacement of nucleoli in response to three cycles of dehydration (Dh) and rehydration (Rh). The shape of the curves stays similar from one cycle to the next and steady state is reached in ~100 seconds. (C) Spatial trajectory of nucleolus 2 from part A in response to three cycles of dehydration and rehydration. The displacements in the *x*-direction are one order of magnitude larger than those in the *y*-direction and therefore the trajectory is essentially one-dimensional and normal to the flow line. (D) The absolute value of displacements of nucleolus 2 scales as shown in Eqn 3. For all dehydration-rehydration cycles, the theoretical curves fit the experimental data well (r^2>0.92). The colours on the graph correspond to those in the spatial trajectory in C.

3B; supplementary material Movie 4, n=10 experiments). This transition from mobile to immobile, taken together with the volume decrease, enables us to use Eqn 1 to estimate the pore radius ξ of the solid phase of cytoplasm:

$$r_{QD} \leq \xi \leq \frac{r_{QD}}{\left(V_{dehyd}/V_0\right)^{1/3}}, \quad (1)$$

where r_{QD} is the radius of the quantum dots. The equation gives $\xi \approx 15$ nm. Consistent with this estimate, larger latex particles (diameter ~50 nm before passivation) passivated with bovine serum albumin (BSA) did not diffuse away from the injection site; whereas smaller ones did (diameter ~25 nm before passivation) (Fig. 3C,D).

When cells containing QDs were locally perfused with hyperosmotic solution, QDs on the perfused side rapidly became immobile, whereas QDs on the unexposed side moved as freely as in untreated cells (Fig. 4A; supplementary material Movie 5). When the external osmotic gradient was removed, QDs on the perfused side started to move freely again within ~10 seconds (Fig. 4B,C; supplementary material Movie 5). We conclude that upon local exposure to an external osmolarity gradient, a hydration gradient is established within the cell that results in the establishment of regions with different pore sizes. Remarkably, these differentially hydrated zones coexisted in a single cell separated by as little as 10 µm.

Water flows across the membrane faster than through the cytoplasm

Experimentally, application or removal of the external osmotic gradient causes the appearance and disappearance of an intracellular strain field in the cytoplasm (Fig. 2B). The establishment and disappearance of this strain field requires fluids to redistribute within the cell and depending on the relative permeability through the cell thickness (cytoplasm and membrane, $\perp$ transverse direction) versus laterally through the cell (cytoplasm only, = lateral direction), water might either diffuse from the hydrated to the dehydrated side or exit the cell through the membrane in response to local application

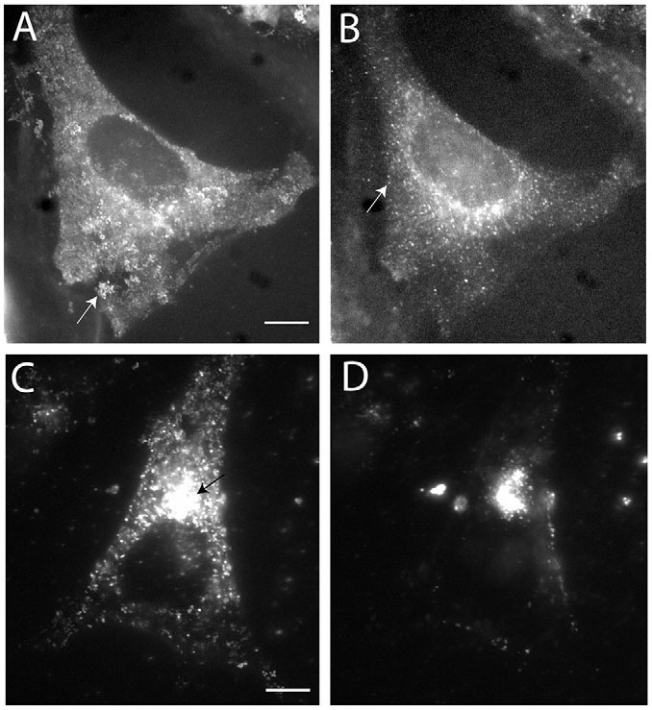

Fig. 3. Movement of quantum dots and latex spheres microinjected in HeLa cells. (A) Projection image of the trajectories of PEG-passivated quantum dots microinjected into HeLa cells in iso-osmotic medium (see supplementary material Movie 3). The quantum dots move rapidly through the cell and their trajectories can be distinguished (arrow). This image is a projection of 200 images representing 40 seconds experimental data. Scale bar: 10 μm. (B) Projection image of the trajectories of quantum dots in the same cell as in A but exposed to hyperosmotic medium (see supplementary material Movie 4). The quantum dots are stationary and therefore each individual quantum dot (arrow) can easily be distinguished. This image is the projection of 200 images representing 40 seconds of experimental data. (C) Localisation of 24-nm diameter BSA-passivated fluorescent latex spheres 10 minutes after microinjection. Beads are present throughout the cell cytoplasm. The point of microinjection is shown by the arrow. Scale bar: 10 μm. (D) Localisation of 50-nm diameter BSA-passivated fluorescent latex spheres 10 minutes after microinjection in the same cell as in C. Because of their larger diameter, beads could not diffuse away from the point of microinjection.

of an external osmotic gradient. Indeed, if the rate of equilibration in the ⊥ direction is slower than that in the = direction, we should be able to detect a transitory convective flow of cytosol from one side of the cell to the other. Conversely, if the rate of equilibration in the ⊥ direction is faster, no flow should be detectable. Experimentally, when local dehydration was removed from cells (supplementary material Movie 5), no convective flow of QDs was observed within the cell and, similarly, when dehydration was applied, no convective flow of QDs could be detected (data not shown). These data suggest that the rate of equilibration in the ⊥ direction is faster than in the = direction. Such a result might be expected on basis of the relative vertical and lateral dimensions of the cell (2 μm height and 50 μm laterally); however, this would imply that water crosses the membrane in response to osmotic forcing faster than it moves through the 2 μm of cytoplasm that constitute the cell height.

As the idea that cytoplasm is more of a barrier to water flow than a membrane is counter-intuitive, we estimated rate of water permeation through these two paths based on published measurements of water permittivity of plasma membranes. Knowing the hydraulic permeability of cytoplasm D, we can compute an equivalent diffusional permeability for a height h of cytoplasm, D/h. Theoretical analysis from our previous work, which was based on an estimated pore size similar to that inferred above, suggests that for HeLa cells $D \approx 0.4\text{-}2.7\ \mu m^2\ second^{-1}$ (Charras et al., 2008), and the cell height is ~2 μm, yielding $D/h \approx 0.2\text{-}1.35\ \mu m\ second^{-1}$. By comparison, the diffusional permeability (P) of water through an animal cell membrane is ~40 μm second^{-1} (Potma et al., 2001). Therefore, we can compare the relative ease with which water crosses the membrane and the cytoplasm by computing the ratio Ph/D, which is ~30-200, suggesting that water permeates more easily across the thin (~6 nm) lipid membrane of the cell than across the whole height of the cytoplasm (~2 μm). The membrane can therefore be ignored at a first approximation and we need to compare the dimensions of the cell in the ⊥ and = directions to compare the rates of equilibration in these directions. The quasi-two-dimensional geometry of the typical spread HeLa cell (~2 μm height vs ~50 μm lateral dimensions) suggests a temporal and spatial separation in scales for processes to equilibrate through-the-cell (⊥ transverse direction) relative to along-the-cell (= lateral direction).

Our theoretical analysis shows that rehydration of the cell should occur preferentially through the cell thickness and that the displacements observed in the hydrated part of the cell result from strain relaxation rather than rehydration. Knowing this, we can utilize experimental observations to estimate the characteristic times for equilibration in the ⊥ and = directions. Since rehydration occurs through the cell thickness, a measure of the half-time for equilibration in the ⊥ direction can be obtained by measuring the half-time of decay in autocorrelation for QD fluorescence intensity after removal of dehydration. Indeed, when the cell is dehydrated, QDs are immobile and autocorrelation is high; whereas when the cell is hydrated, QDs can move around freely and autocorrelation is low. Therefore, the transition time from a high autocorrelation to a low autocorrelation corresponds to the time needed for the pore size of the solid phase to increase to a size larger than the diameter of a QD. This was observed experimentally: when the cytoplasm rehydrated, QD motion restarted and autocorrelation in QD fluorescence intensity decreased. In our experiments, the half-time for rehydration, τ_w, was ~8±4 seconds (Fig. 4C, n=29 regions from 18 cells), consistent with other temporal measurements of change in cell volume (Lucio et al., 2003). Strain relaxation occurs in the = direction and therefore the half-time for equilibration (τ_s) in the = direction can be estimated by tracking the displacement of cellular nucleoli as they relax after removal of the external osmotic gradient. Experimentally, we find $\tau_s \approx 26 \pm 16$ seconds (n=86 nucleoli from 45 cells) (Fig. 5C,D). τ_w was significantly smaller than τ_s (P<0.001), confirming experimentally that equilibration in the ⊥ direction is fast compared to equilibration in the = direction.

Based on these results and the motion of QDs during the transitory regime, we infer the existence of three regions in the perfused cell at steady state (Fig. 1B): Region 1 in the hydrated, unexposed region, where the cell is in osmotic and mechanical equilibrium with its environment; region 2 in the osmotically stressed region, where the cell is dehydrated and thus shrinks both laterally and vertically; region 3 might exist inside the cell where water continuously moves from the hydrated to the dehydrated region, and would be analogous to the transition zone determined by the balance between convection and diffusion outside the cell. However, further experimental work will be needed to test the presence of this latter region.

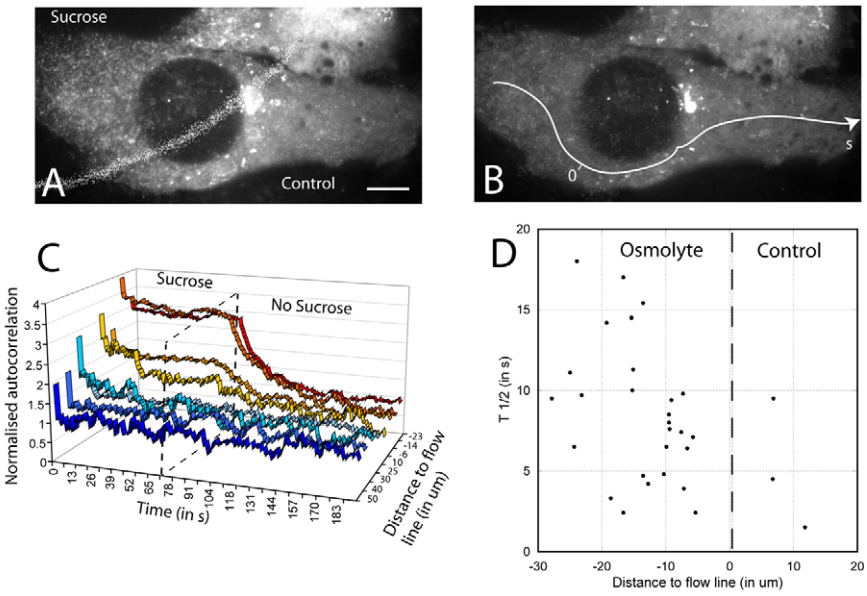

Fig. 4. Distinct hydraulic environments separated by ~10 µm can coexist within a cell. (A) Fluorescence image of a HeLa cell microinjected with PEG-passivated quantum dots and locally exposed to a hyperosmotic solution. This image is a projection of 99 images representing 70 seconds. The quantum dots in the dehydrated region (sucrose) are immobile and therefore distinctly visible. Quantum dots on the fully hydrated side (control) are highly mobile and therefore not as distinctly visible (see supplementary material Movie 5). Hence, two different hydraulic regimes separated by only a few µm can coexist within the cell, presumably due to rapid equilibration across the membrane in the vertical direction. Scale bar: 10 µm. (B) Fluorescence image of the same cell as in A but after the dehydration has been removed. This image is the projection of 140 time points corresponding to 110 seconds. Quantum dots cannot be as easily distinguished as in A because the immobile quantum dots have regained mobility. *s* is the curvilinear distance along the line, with 0 corresponding to the point of transition between the dehydrated and hydrated parts of the cell. (C) Normalised autocorrelation function for regions along the line shown in B. In areas where the quantum dots move very little (i.e. in the dehydrated zone, for $s<0$), the autocorrelation coefficient is high and decreases when dehydration is removed. In areas where the quantum dots are highly mobile ($s>0$), the autocorrelation coefficient is low and remains low after removal of dehydration. The colours indicate the distance of the region examined along the line drawn in B. Regions with a negative curvilinear abscissa appear in hot colours with red being the furthest corresponding to the dehydrated part of the cell. Regions with a positive abscissa appear in blue with darker blue being further away from the zero. These correspond to hydrated parts of the cell. (D) Half-time of decay in autocorrelation function after removal of dehydration as a function of the distance to the flow boundary. Recovery half-times are not correlated with distance to the flow boundary (30 measurements on 18 cells).

A minimal scaling theory

Taken together, our experiments allow us to infer the existence of relative movement between the cytoskeleton and interstitial fluid in response to localized application of osmotic stresses. The simplest model of the cytoplasm consistent with these observations is that of a soft, porous fluid-filled sponge. This model can be described using the theory of poroelasticity, an inherently multi-phase description that is qualitatively different from most previous models that infer a single-phase viscoelastic or viscoplastic cytoplasm. On length-scales large compared to the scale that characterizes the pore radius ξ (Fig. 1A), the cytoplasm can be viewed as a fluid-solid mixture in which there can be relative motion between the two phases. Here, as a first approximation, we derive simple predictions at the scaling level to test whether our experimental results can be explained in the framework of poroelasticity.

The constitutive equations for poroelastic media have been derived many times [e.g. see the textbook by Wang (Wang, 2000)] and lead to a linear diffusion equation for the dilatational strain, or equivalently for the volumetric fluid content in the medium, with a diffusion constant D (Wang, 2000) and yield:

$$E(\varphi)\Delta u_{=} = \frac{1}{k}\partial_t u_{=} \text{ or } D\Delta u_{=} - \partial_t u_{=} = 0\ , \qquad (2)$$

with $u_{=}$ being the lateral displacements and k the hydraulic permeability of the cytoplasm; $D{=}E(\varphi)k$ with $E(\varphi)$ being the bulk modulus of the solid phase for a fluid fraction φ.

In the framework of poroelasticity, the time-dependent properties of the cytoplasm can be expressed in terms of a few effective parameters such as the mesh porosity ξ, the interstitial fluid viscosity μ and the elasticity of the constituent solid network E_f. At a scaling level, a simple relationship for k follows by assuming that the fluid phase moves through pores of radius ξ in response to a pressure gradient and this yields $k{\approx}\xi^2/\mu$, with μ being the cytosolic viscosity (Charras et al., 2008). The cytoskeleton is the main contributor to cell elasticity and the network bulk modulus scales as $E{\approx}E_f(1{-}\varphi)^{\alpha}$, where the exponent $\alpha{\in}[1.5,2.5]$, depending on the microscopic model chosen for the cytoskeletal network (e.g. enthalpic cellular solid, entropic chain, worm-like chain etc.) (Gardel et al., 2004).

In our experiments, the applied osmotic forces lead to a displacement of the cytoplasm-membrane system imposed at the boundary between the dehydrated and hydrated zones. Since equilibration in the $\perp$ direction is rapid compared to that in the = direction, rapid removal of the hyperosmotic medium is equivalent to imposing a step displacement onto the dehydrated part of the cell. Therefore, as a first approximation, nucleolar displacements at a distance x from the dehydrated zone (Fig. 1A) should scale as the solution of the diffusion Eqn 2 for a step change in applied displacement on part of the cell and this is given by:

$$u_{=}(x,t) \approx erfc\left(\frac{x}{\sqrt{4Dt}}\right), \qquad (3)$$

with t being the time from the start of rehydration (Wang, 2000). For application of hyperosmotic medium, the solution is of the same form but with scales as an error function (*erf*) instead of a complementary error function (*erfc*). We use this simple theoretical solution to fit experimentally measured nucleolar displacements in response to application or removal of hyperosmotic medium (Fig. 2D) using D as a fitting parameter. We note that this simple Green's function approach to the problem ignores the complications associated with boundary conditions that will in general lead to exponential-type solutions; our estimates are reasonable at short times but clearly deviate from experimental observations at intermediate and long times (which was ~500 seconds with the numerical values in this study) when the effects of finite cell size become important (Mitchison et al., 2008).

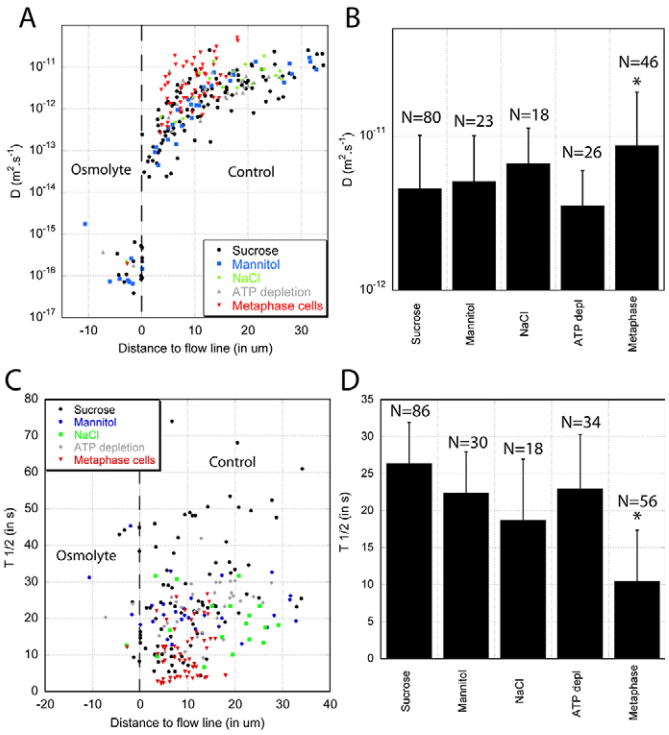

Fig. 5. Stress diffusion constant and half-time of recovery in response to different treatments. (A) Stress diffusion constant as a function of distance to the boundary between hydrated and dehydrated zones for different conditions. The stress diffusion constant increases as a function of distance away from the boundary, probably reflecting a gradient in pore size due to partial dehydration, and reaches a plateau for distances superior to 5 µm. Metaphase cells did not cluster with the rest of the data. (B) Average stress diffusion constant for distances from the boundary superior to 5 µm for different treatments. Stress diffusion constants for different osmolytes are not significantly different (P>0.08). The stress diffusion constant in ATP-depleted cells is not significantly different from that of live cells (P=0.18). Metaphase cells had a twofold larger stress diffusion constant than interphase cells (*P=0.002). The number of data points for each treatment appears above the column. Error bars denote standard deviations. (C) Half-time of recuperation after dehydration as a function of distance to the flow boundary. The half-time of recuperation did not show any correlation with spatial location. Metaphase cells did not cluster with the rest of the data. (D) Average half-time of recovery for different treatments. Recovery half-times were not significantly different for different osmolytes (P>0.025). Recovery half-time for ATP-depleted cells was not significantly different from that for live cells (P=0.11). The half-time of recovery for metaphase cells was significantly smaller than for interphase cells (sucrose, *P<0.001).

Experimental strain relaxation is well-described in the framework of poroelasticity

Over short times (~120 seconds), the experimental data was well fit by Eqn 3 (Fig. 2D) and a total of 256 experimental nucleolar displacement curves from 100 cells were fit with an average $r^2 \approx 0.96 \pm 0.05$, directly confirming that cytomechanics can be well-described by poroelasticity. Data points for different osmolytes clustered together, confirming the generality of the phenomenon (Fig. 5A,B); the mean poroelastic diffusion constant (D) for interphase HeLa cells was ~5±5 µm^2 second^{-1} (n=80 nucleoli from 47 cells). Since the poroelastic diffusion constant D is a function of the pore structure, which is variable, we plotted D as a function of the distance to the dehydration zone (Fig. 5A), and see a clear transition zone of order O (5 µm) in which D increased before reaching a plateau. This suggested that a gradient in hydration, and therefore in pore size, might exist within the cytoplasm away from the dehydrated region. Such a gradient in hydration might be indicative of the existence of the steady-state transition zone inferred in region 3 (Fig. 1).

To determine whether the observed response was due to passive physical effects rather than active biochemical ones, we pretreated the cells for 20 minutes with an energy poison (NaN_3 and 2-deoxy-glucose) that depleted cellular ATP. We found that this had no effect on the mechanical response (Fig. 5B) (D, n=26 nucleoli from 11 cells, $p_{\text{ATP depletion/sucrose}}$=0.2), consistent with a simple poroelastic interpretation of our results in terms of the passive structural, mechanical and hydraulic properties of cytoplasm over the time-scales of our experiments. Over much longer time-scales, when the cell can alter its cytoskeletal organization dramatically, we expect D to change. To test the influence of cytoskeletal organization on the poroelastic diffusion constant, we carried out similar experiments in mitotic cells blocked in metaphase by overnight treatment with 100 nM nocodazole. During metaphase in control cells, F-actin and vimentin intermediate filaments concentrate in a shell at the cell periphery (Alberts et al., 2008) (Fig. 6E,F), microtubules reorganize to form the mitotic spindle (Fig. 6A,B,E,F), and cytokeratin filaments disassemble (Windoffer and Leube, 1999) (Fig. 6A,B). In cells blocked in metaphase by overnight nocodazole treatment, actin concentrated at the cortex as in control cells (data not shown), the mitotic spindle was absent but some microtubules subsisted in close association with the chromosomes, and the cytokeratin and vimentin intermediate filaments concentrated at the cell cortex (Fig. 6C,D,G,H). Therefore, the cytoplasm of HeLa cells blocked in metaphase with nocodazole is depleted of cytoskeletal fibers relative to an interphase cell. D in mitotic cells was twice as large as in interphase cells (n=46 fiduciary marks tracked from 20 cells, $p_{\text{metaphase cells/interphase cells}}$<0.01), showing that D is indeed sensitive to the state of cytoskeletal organization. The fact that D did not change more in mitosis suggests that other factors, such as macromolecular crowding, might also participate in restricting water flow rates.

Discussion

Experimental evidence of the time-dependent mechanical properties of cells abounds and earlier efforts to model the dynamics of cells assumed that cells were viscoelastic (Bausch and Kroy, 2006; Boal, 2002). Most experimental studies examining these properties interpret their results either in terms of rheological models with a dissipation and a storage modulus or in terms of phenomenological models relying on Kelvin, Voigt or standard linear models (Bausch et al., 1999; Mahaffy et al., 2000). Both of these approaches have been used successfully to fit experimental data from a wide variety of cell types; however, they suffer from two shortfalls. First, understanding the relationship between the rheological parameters and the cell ultrastructure is non-trivial. Second, these models do not account for the fact that the cytoplasmic fluid can move separately from the cytoplasmic solid fraction. By contrast, our experimental results suggest that water movements need to be considered to understand the dynamic mechanical behavior of cells. This implies that theoretical understanding of the cytoplasmic dynamics of animal cells requires a theory that accounts for the fluid and solid phases that interpenetrate each other. We show that poroelasticity (Biot, 1941) can be utilized to describe such materials, and interpret our experimental results regardless of the osmolyte used, the stage of the cell cycle, or even whether the cell was alive or not. Our results emphasize the need for measurements that

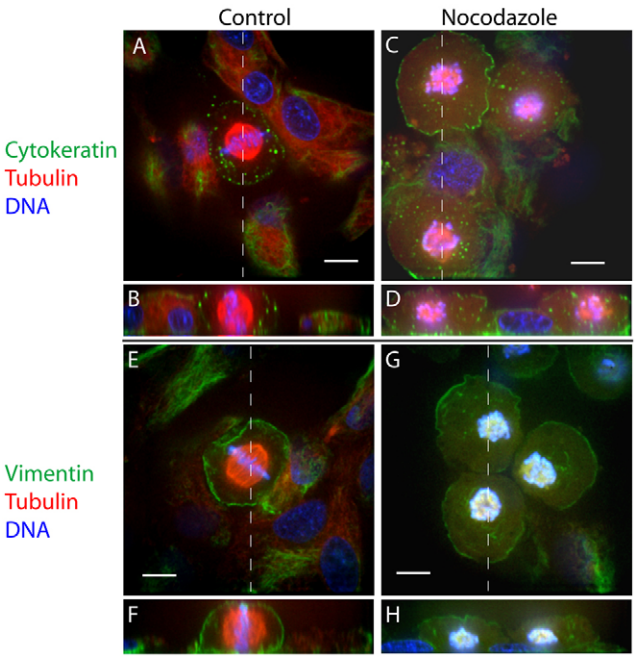

Fig. 6. Vimentin, cytokeratin, tubulin and nucleic acid distributions during metaphase in control and nocodazole-treated HeLa cells. Cytokeratin 18 (A-D) and vimentin (E-H) are in green, microtubules in red, and nucleic acids in blue. Images A,C,E,G are single confocal sections. Images B,D,F,H are cross-sections of the confocal stacks along the dashed line in A,C,E,G, respectively. (A,B) During metaphase, cytokeratin redistributes to the cell periphery and microtubules form the mitotic spindle. (C,D) In cells blocked in metaphase by overnight treatment with nocodazole, the mitotic spindle is absent though some microtubules subsist in between the chromosomes. As in control cells, the cytokeratin redistributes to the cell periphery. (E,F) During metaphase, vimentin redistributes to the cell periphery and microtubules form the mitotic spindle. (G,H) In cells blocked in metaphase by overnight treatment with nocodazole, the mitotic spindle is absent. As in control cells, vimentin redistributes to the cell periphery. Scale bars: 10 μm.

challenge the cytoplasm, by making the fluid phase flow relative to the solid network, if we are to understand the mechanical nature of cytoplasm.

In addition to providing a minimal model that is consistent with the observed phenomena, poroelastic theory also naturally relates microscopic measurable parameters to mesoscopic observables. Indeed, simple scaling arguments suggest that the diffusion constant D depends on three measurable physical parameters (Charras et al., 2008):

$$D \approx \frac{E\xi^2}{\mu} ,$$

with E being the elasticity of the solid phase, μ the viscosity of the cytosol, and ξ the pore radius of the solid phase. Previous experimental and theoretical work has shown that the cytoskeleton ultrastructure plays a crucial role in setting the elasticity E of gels of cytoskeletal proteins (Gardel et al., 2006; Gardel et al., 2004). In living cells, it is well-established that the cytoskeleton (and in particular actomyosin) accounts for most of the measured cellular elasticity (Martens and Radmacher, 2008; Rotsch and Radmacher, 2000; Ting-Beall et al., 1995; Tsai et al., 1994). Although we show that the cytoskeleton also plays a role in modulating the time-dependent mechanical properties of the cell, it is unclear how it does so. The pore diameter (~30 nm) that we estimated from QD trapping is consistent with other experimental measurements of the pore size in cultured cells (Luby-Phelps et al., 1987), but is smaller than that observed in electron micrographs of cytoskeletal networks alone (Hartwig, 1986; Heuser and Kirschner, 1980), except in the lamellipodium where very high concentrations of actin filaments are present (Svitkina et al., 1997). Furthermore, our experiments showed that metaphase cells treated with nocodazole still displayed poroelastic properties despite the absence of cytoskeletal fibers within the cytoplasm.

Taken together, these data suggest that macromolecular crowding might play an important role in cell hydraulics and that the experimentally determined pore diameter might result from a combination of cytoskeletal pore size and intra-pore crowding by macromolecular mobile elements such ribosomes or lipid vesicles (Medalia et al., 2002) (Fig. 1). Indeed, in transmission electron micrographs of cells dehydrated in hyperosmotic medium, large numbers ribosomes appear tightly packed between cytoskeletal fibers, lipid vesicles, and mitochondria (Albrecht-Buehler and Bushnell, 1982). One intriguing consequence of the poroelastic nature of cells is that modulating E, μ and ξ might provide an efficient means for the cell to biochemically modulate its rheological properties spatially and temporally.

Although our study shows that poroelasticity can successfully account for the observed behavior of HeLa cells in response to localized dehydration, it represents a preliminary study and many questions still remain to be answered. First, meaningful comparisons between the experimentally measured strain diffusion constant D and theoretical estimates are difficult at best owing to the range of experimental measurements reported for E and μ. Experimental measures of the elastic modulus of cells can be obtained through a variety of techniques [e.g. atomic force microscopy (AFM) microindentation, bead-twisting rheology etc.] but these yield very spatially heterogeneous values [varying between 0.1 and 100 kPa, depending on subcellular location with AFM (Charras and Horton, 2002; Radmacher, 1997)], and the measured elastic moduli vary from technique to technique, even for the same cell type [$E_{\mathrm{AFM}} \approx 2$ kPa (Charras et al., 2005), $E_{\mu\mathrm{rheology}} \approx 200$Pa (Coughlin et al., 2006) for M2 melanoma cells]. Furthermore, the reported experimental estimates for the viscosity of the cytosol vary between $\mu \approx 3 \times 10^{-3}$ and 10^{-1} Pa second [for small fluorophores (Mastro et al., 1984) and for actin monomers (Kreis et al., 1982), respectively]. Therefore, any estimate for D based on theoretical predictions would span several orders of magnitude, rendering comparison with experimental values meaningless.

Second, it remains to be determined whether poroelasticity can be used to describe the mechanics of a wide variety of cell types as well as rheological models do. Indeed, the time-dependent properties of the cytoplasm of some cell types might be better fit using other theoretical formulations. This could especially be the case for cells with a low cytoskeleton density, such as eggs, which might be better described as viscous liquids (Daniels et al., 2006).

Third, on the basis of the difference in length scales between the directions (~25 μm), we would expect the time scales for fluid equilibration in the ⊥ and = directions to scale accordingly. By contrast, our experimental results show that water equilibration in the ⊥ direction is only threefold faster than in the = direction. This unexpectedly small difference might be due to the presence of a dense layer of submembranous actin (the cortex), which would slow ⊥ equilibration but not = equilibration. Indeed, experiments examining the diffusion of deuteriated water into *Dictyostelium* cells have shown the presence of a zone of restricted water diffusion

below the membrane of these cells, coincident with the presence of a dense actin cortex (Potma et al., 2001).

Fourth, one of the predictions of our simple scaling law is that the cytoskeleton strongly impacts the strain diffusion constant by setting both the mesh size and the elasticity of the cell. Experiments relying on the selective depolymerization of the different cytoskeletal components will be needed to assess their involvement in setting cytoplasmic strain diffusion. Indeed, experiments using micropipette aspiration to determine cell viscosity suggest that disrupting actin filaments leads to a sharp decrease in viscosity (Ting-Beall et al., 1995; Tsai et al., 1994). In addition, as the cytoskeletal ultrastructure and elasticity are spatially heterogenous, cellular viscosity and strain diffusion should also be spatially heterogeneous with zones of high cytoskeletal density having a lower strain diffusion constant and a higher viscosity.

In conclusion, poroelasticity provides a unifying framework for the interpretation of experiments on the time-dependent mechanical properties of cells in the context of motility, morphogenesis and division. Simple estimates show that the relative importance of cell hydraulics and cytoskeletal dynamics depends on the time-, length- and force-scales involved. In this picture, cellular morphodynamics can be described by the mechanics and hydraulics of the cytoskeletal mesh structure, the membrane permeability, local contractility and adhesion. Modulation of one or more of these parameters locally could give rise to heterogeneities in cellular hydraulics, and these heterogeneities might be exploited by cells to locomote and modulate their time-dependent mechanical properties.

Materials and Methods

Cell culture

HeLa cells were cultured in DMEM (Invitrogen, Carlsbad, CA) with penicillin streptomycin and 10% fetal calf serum (FCS). For metaphase arrest, cells were incubated overnight in culture medium supplemented with 100 nM nocodazole (Sigma, St Louis, MO). Before experimentation, the cells were detached from the culture dish by enzymatic digestion with trypsin-EDTA, plated onto glass coverslips, and cultured overnight. For laminar flow experiments, Leibovitz L15 medium (Invitrogen) supplemented with 10% FCS was used instead of DMEM.

Microscopy

All imaging was done on a Nikon TE-2000 inverted microscope (Nikon, Yokohama, Japan). Both a 100× 1.3 NA oil immersion objective and a 20× objective were used for imaging. Fluorophores were excited with epifluorescence illumination and the appropriate filter sets. Quantum dots were excited with a specific filter (E460SPUVv2, Chroma, Rockingham, VT), which has a peak at 400 nm. Images were captured on an Orca ER CCD camera (Hamamatsu, Hamamatsu, Japan) and acquired on a PC using Metamorph software (Molecular Devices, Sunnyvale, CA). For display, images were low-pass filtered and scaled such that background fluorescence was minimal. In some cases, projection images were created by projecting the maximal intensity of fluorescence at several time points onto one image.

Image processing

For easier visualization, flow lines delineating the boundary between the zone exposed to sucrose and the control zone were superimposed onto the DIC images using Metamorph. To do this, fluorescence images of the flow tracer were thresholded and intensities of 50% of the maximum intensity were converted to a binary image that was inverted and superimposed onto the DIC image using an OR operator. Nucleolus tracking was effected by defining a rectangular region of interest around the nucleolus and using the track function in Metamorph. The data was output to Excel (Microsoft, Redmond, WA) and the relative displacement compared to the origin was computed for each nucleolus.

Local perfusion

Local treatment of cells was performed as described previously (Charras et al., 2005). Briefly, a laminar flow of medium was established in the flow chamber. The tip of a micropipette containing sucrose and a fluorescent tracer were brought into the vicinity of the cell to be treated with a micromanipulator (Narishige, Tokyo, Japan) and the position was adjusted such that the fluorescent tracer only bathed one half of the cell. During the experiment, images were acquired at 0.5-, 1-, or 5-second intervals using DIC illumination and 488 or 568 nm excitation to visualize the cells and the fluorescent tracer, respectively. For experiments necessitating frame rates higher than 1 Hz, we adjusted the micropipette such that one third of the cell was exposed to sucrose, waited two minutes for equilibration, acquired a fluorescence image to visualise the flow boundary, started DIC acquisition, removed dehydration and made note of the frame, and finally followed relaxation.

Microinjection and analysis of quantum dot movement

Microinjections were performed as described previously (Charras et al., 2006). PEG-passivated 565 quantum dots or BSA-passivated fluorescent latex microspheres (Invitrogen) were diluted in injection buffer (50 mM potassium glutamate, 0.5 mM $MgCl_2$, pH 7.0) to achieve a final concentration of 0.1 μM. To qualitatively visualize the extent of quantum dot movement, time series were projected onto one plane using Metamorph. Autocorrelation functions were computed using custom-written software running under Pv-wave (Visual Numerics, Houston, TX). Briefly, the metamorph stack file was read into the software and the user chose several rectangular regions situated both in the dehydrated zone and the hydrated zone. The software then calculated the intensity autocorrelation of each region with its intensity at time t=0 for all time points. The calculated autocorrelations were then normalized to the average value of the autocorrelation when the region was fully hydrated. Half-times were computed using Excel.

Measurement of cell volume and estimation of volume change in response to hyperosmotic shock

To measure change in volume in response to osmotic shock, HeLa cells cultured overnight on glass coverslips were loaded with the cytoplasmic indicator CMFDA (Molecular Probes) for 30 minutes at 37°C prior to experimentation. The volume of the cells was estimated by acquiring optical sections through the cells at 0.5 μm intervals with a confocal microscope (FV1000, Olympus, Tokyo, Japan) before and after exposure to a 300 mM sucrose solution dissolved in growth medium. The area of each optical section was estimated as described previously (Charras et al., 2005).

Immunostaining

Cells for immunostaining were plated on glass coverslips two days prior to fixation. For metaphase block experiments, 100 nM nocodazole was added to the cells the day before fixation. Cells were fixed with a 50:50 mix of acetone and methanol at –20°C. After passivation with a solution of 10 mg ml^{-1} BSA in PBS (PBS-BSA), the cells were stained for 1 hour with polyclonal anti-α tubulin (1:10 dilution; Abcam, Cambridge, UK), and either monoclonal anti-cytokeratin 18 (1:100 dilution; Abcam) or monoclonal anti-vimentin (1:100 dilution; Sigma, St Louis, MO). The coverslips were washed with PBS-BSA and stained with goat-anti mouse fluorescein isothiocyanate (FITC) and swine anti-rabbit tetramethylrhodamine-5-isothiocyanate (TRITC) (both 1:40 dilution; Dako, Denmark). After further washes in PBS-BSA, the cells were stained with 1 μg ml^{-1} Hoechst 33342 for 10 minutes (Invitrogen). The cells were examined on a spinning disk confocal (Andor, Belfast, UK) with the appropriate laser excitations for Hoechst 33342, FITC and TRITC (405 nm, 488 nm and 568 nm, respectively).

Data analysis and curve fitting

Curve fitting data, half-time data and trajectory data were analyzed using Excel (Microsoft) and Kaleidagraph (Synergy software, Reading, PA). Curve fitting was effected in the log-linear scale to minimise the influence of prefactors using Kaleidagraph (Synergy software). Some uncertainty as to when movement experimentally begins was accommodated by replacing t with $(t–t_0)$, with t_0 being the first time point, and fitting for t_0 and the stress diffusion constant D (see theory in the results section). Goodness of fit was assessed using the r^2 value. The distance x of each nucleolus to the flow line was measured using Metamorph and was set as a constant in the fit. For nucleoli within the dehydrated zone, the distance to the flow line was arbitrarily set to 0.1 μm.

Statistics

Diffusion constants and relaxation times were compared using a Student's t-test and we considered differences significant for P<0.01.

G.T.C. is in receipt of a University Research Fellowship from the Royal Society, L.M. acknowledges the support of Harvard University and T.J.M. acknowledges the support of the NIH. G.T.C. wishes to acknowledge the UCL Comprehensive Biomedical Research Centre for generous funding of microscopy equipment. Deposited in PMC for release after 12 months.

References

Alberts, B., Bray, D., Lewis, J., Raff, M., Roberts, K. and Watson, J. (2008). *Molecular Biology of the Cell*. New York: Garland.

Albrecht-Buehler, G. and Bushnell, A. (1982). Reversible compression of cytoplasm. *Exp. Cell Res.* **140**, 173-189.

Allen, R. D. and Roslansky, J. D. (1959). The consistency of ameba cytoplasm and its bearing on the mechanism of ameboid movement. I. An analysis of endoplasmic velocity profiles of Chaos (L.). *J. Biophys. Biochem. Cytol.* **6**, 437-446.
Bausch, A. R. and Kroy, K. (2006). A bottom-up approach to cell mechanics. *Nat. Phys.* **2**, 231-238.
Bausch, A. R., Moller, W. and Sackmann, E. (1999). Measurement of local viscoelasticity and forces in living cells by magnetic tweezers. *Biophys. J.* **76**, 573-579.
Biot, M. (1941). General theory of three-dimensional consolidation. *J. Appl. Phys.* **12**, 155-164.
Boal, D. H. (2002). *Mechanics of the Cell*. Cambridge: Cambridge University Press.
Chandler, D. (2002). Hydrophobicity: two faces of water. *Nature* **417**, 491.
Chandran, P. L. and Barocas, V. H. (2004). Microstructural mechanics of collagen gels in confined compression: poroelasticity, viscoelasticity, and collapse. *J. Biomech. Eng.* **126**, 152-166.
Charras, G. T. and Horton, M. A. (2002). Determination of cellular strains by combined atomic force microscopy and finite element modeling. *Biophys. J.* **83**, 858-879.
Charras, G. T., Yarrow, J. C., Horton, M. A., Mahadevan, L. and Mitchison, T. J. (2005). Non-equilibration of hydrostatic pressure in blebbing cells. *Nature* **435**, 365-369.
Charras, G. T., Hu, C. K., Coughlin, M. and Mitchison, T. J. (2006). Reassembly of contractile actin cortex in cell blebs. *J. Cell Biol.* **175**, 477-490.
Charras, G. T., Coughlin, M., Mitchison, T. J. and Mahadevan, L. (2008). Life and times of a cellular bleb. *Biophys. J.* **94**, 1836-1853.
Coughlin, M. F., Puig-de-Morales, M., Bursac, P., Mellema, M., Millet, E. and Fredberg, J. J. (2006). Filamin-a and rheological properties of cultured melanoma cells. *Biophys. J.* **90**, 2199-2205.
Daniels, B. R., Masi, B. C. and Wirtz, D. (2006). Probing single-cell micromechanics in vivo: the microrheology of C. elegans developing embryos. *Biophys. J.* **90**, 4712-4719.
Dembo, M. and Harlow, F. (1986). Cell motion, contractile networks, and the physics of interpenetrating reactive flow. *Biophys. J.* **50**, 109-121.
Denker, S. P. and Barber, D. L. (2002). Cell migration requires both ion translocation and cytoskeletal anchoring by the Na-H exchanger NHE1. *J. Cell Biol.* **159**, 1087-1096.
Derfus, A. M., Chan, W. C. W. and Bhatia, S. N. (2004). Intracellular delivery of quantum dots for live cell labeling and organelle tracking. *Adv. Mater.* **16**, 961-966.
Gardel, M. L., Shin, J. H., MacKintosh, F. C., Mahadevan, L., Matsudaira, P. and Weitz, D. A. (2004). Elastic behavior of cross-linked and bundled actin networks. *Science* **304**, 1301-1305.
Gardel, M. L., Nakamura, F., Hartwig, J. H., Crocker, J. C., Stossel, T. P. and Weitz, D. A. (2006). Prestressed F-actin networks cross-linked by hinged filamins replicate mechanical properties of cells. *Proc. Natl. Acad. Sci. USA* **103**, 1762-1767.
Gu, W. Y., Lai, W. M. and Mow, V. C. (1997). A triphasic analysis of negative osmotic flows through charged hydrated soft tissues. *J. Biomech.* **30**, 71-78.
Harold, F. M. (2002). Force and compliance: rethinking morphogenesis in walled cells. *Fungal Genet. Biol.* **37**, 271-282.
Hartwig, J. H. (1986). Actin filament architecture and movements in macrophage cytoplasm. *Ciba Found. Symp.* **118**, 42-53.
Herant, M., Marganski, W. A. and Dembo, M. (2003). The mechanics of neutrophils: synthetic modeling of three experiments. *Biophys. J.* **84**, 3389-3413.
Heuser, J. E. and Kirschner, M. W. (1980). Filament organization revealed in platinum replicas of freeze-dried cytoskeletons. *J. Cell Biol.* **86**, 212-234.
Hui, C. Y. and Muralidharan, V. (2005). Gel mechanics: a comparison of the theories of Biot and Tanaka, Hocker, and Benedek. *J. Chem. Phys.* **123**, 154905.
Keren, K., Pincus, Z., Allen, G. M., Barnhart, E. L., Marriott, G., Mogilner, A. and Theriot, J. A. (2008). Mechanism of shape determination in motile cells. *Nature* **453**, 475-480.
Kreis, T. E., Geiger, B. and Schlessinger, J. (1982). Mobility of microinjected rhodamine actin within living chicken gizzard cells determined by fluorescence photobleaching recovery. *Cell* **29**, 835-845.
Luby-Phelps, K., Castle, P. E., Taylor, D. L. and Lanni, F. (1987). Hindered diffusion of inert tracer particles in the cytoplasm of mouse 3T3 cells. *Proc. Natl. Acad. Sci. USA* **84**, 4910-4913.
Lucio, A. D., Santos, R. A. and Mesquita, O. N. (2003). Measurements and modeling of water transport and osmoregulation in a single kidney cell using optical tweezers and videomicroscopy. *Phys. Rev. E Stat. Nonlin. Soft Matter Phys.* **68**, 041906.
Mahaffy, R. E., Shih, C. K., MacKintosh, F. C. and Kas, J. (2000). Scanning probe-based frequency-dependent microrheology of polymer gels and biological cells. *Phys. Rev. Lett.* **85**, 880-883.
Martens, J. C. and Radmacher, M. (2008). Softening of the actin cytoskeleton by inhibition of myosin II. *Pflugers Arch.* **456**, 95-100.
Mastro, A. M., Babich, M. A., Taylor, W. D. and Keith, A. D. (1984). Diffusion of a small molecule in the cytoplasm of mammalian cells. *Proc. Natl. Acad. Sci. USA* **81**, 3414-3418.
Medalia, O., Weber, I., Frangakis, A. S., Nicastro, D., Gerisch, G. and Baumeister, W. (2002). Macromolecular architecture in eukaryotic cells visualized by cryoelectron tomography. *Science* **298**, 1209-1213.
Mitchison, T. J., Charras, G. T. and Mahadevan, L. (2008). Implications of a poroelastic cytoplasm for the dynamics of animal cell shape. *Semin. Cell Dev. Biol.* **19**, 215-223.
Pons, T., Uyeda, H. T., Medintz, I. L. and Mattoussi, H. (2006). Hydrodynamic dimensions, electrophoretic mobility, and stability of hydrophilic quantum dots. *J. Phys. Chem. B* **110**, 20308-20316.
Potma, E., de Boeij, W. P., van Haastert, P. J. and Wiersma, D. A. (2001). Real-time visualization of intracellular hydrodynamics in single living cells. *Proc. Natl. Acad. Sci. USA* **98**, 1577-1582.
Radmacher, M. (1997). Measuring the elastic properties of biological samples with the AFM. *IEEE Eng. Med. Biol. Mag.* **16**, 47-57.
Rosenbluth, M. J., Crow, A., Shaevitz, J. W. and Fletcher, D. A. (2008). Slow stress propagation in adherent cells. *Biophys. J.* **95**, 6052-6059.
Rotsch, C. and Radmacher, M. (2000). Drug-induced changes of cytoskeletal structure and mechanics in fibroblasts: an atomic force microscopy study. *Biophys. J.* **78**, 520-535.
Saadoun, S., Papadopoulos, M. C., Hara-Chikuma, M. and Verkman, A. S. (2005). Impairment of angiogenesis and cell migration by targeted aquaporin-1 gene disruption. *Nature* **434**, 786-792.
Svitkina, T. M., Verkhovsky, A. B., McQuade, K. M. and Borisy, G. G. (1997). Analysis of the actin-myosin II system in fish epidermal keratocytes: mechanism of cell body translocation. *J. Cell Biol.* **139**, 397-415.
Tanaka, T., Hocker, L. O. and Benedek, G. B. (1973). Spectrum of light scattered from a viscoelastic gel. *J. Chem. Phys.* **59**, 5151-5159.
Theriot, J. A., Mitchison, T. J., Tilney, L. G. and Portnoy, D. A. (1992). The rate of actin-based motility of intracellular Listeria monocytogenes equals the rate of actin polymerization. *Nature* **357**, 257-260.
Tilney, L. G., Connelly, P. S. and Portnoy, D. A. (1990). Actin filament nucleation by the bacterial pathogen, Listeria monocytogenes. *J. Cell Biol.* **111**, 2979-2988.
Ting-Beall, H. P., Lee, A. S. and Hochmuth, R. M. (1995). Effect of cytochalasin D on the mechanical properties and morphology of passive human neutrophils. *Ann. Biomed. Eng.* **23**, 666-671.
Tsai, M. A., Frank, R. S. and Waugh, R. E. (1994). Passive mechanical behavior of human neutrophils: effect of cytochalasin B. *Biophys. J.* **66**, 2166-2172.
Wang, H. (2000). *Theory of Linear Poroelasticity with Applications to Geomechanics and Hydrogeology*. Princeton, NJ: Princeton University Press.
Windoffer, R. and Leube, R. E. (1999). Detection of cytokeratin dynamics by time-lapse fluorescence microscopy in living cells. *J. Cell Sci.* **112**, 4521-4534.
Zicha, D., Dobbie, I. M., Holt, M. R., Monypenny, J., Soong, D. Y., Gray, C. and Dunn, G. A. (2003). Rapid actin transport during cell protrusion. *Science* **300**, 142-145.

Journal of Cell Science